Failure mechanics in elastomer toughened polypropylene

J. Jancar*, A. DiAnselmo† and A. T. DiBenedetto
Institute of Materials Science, University of Connecticut, Storrs, CT 06268, USA

and J. Kucera
Research Institute of Macromolecular Chemistry, Tkalcovska 2, 65649 Brno, Czechoslovakia
(Received 10 July 1991; revised 10 June 1992)

Dynamic mechanical, tensile and impact properties and modes of failure of binary blends of polypropylene and ethylene-propylene random copolymer rubber (PP/EPR) were studied over a wide interval of EPR volume fractions. The effect of grafting maleic anhydride on both PP and EPR on the mechanical properties was also investigated. The effects of elastomer inclusions on the failure processes were analysed in terms of critical strain energy release rate and Charpy notched impact strength (NIS). Phase morphology of the blends was examined using dynamic mechanical spectroscopy and SEM. PP remains as a continuous phase even as a minor component. This is reflected by the experimental values of elastic moduli significantly higher than those predicted using the Kerner model. The plane strain and plane stress limits of the critical strain energy release rate for initiation of cracks in the blends were the same as those for neat PP. On the other hand, the presence of EPR decreased the yield strength of the material due to the overlapping stress fields of adjacent particles, thereby increasing significantly the critical strain energy release rate for crack propagation. This was reflected by an increase in NIS. The results are explained in terms of a mixed mode of fracture with macroscopic transition from the state of plane strain to plane stress.

(Keywords: polypropylene; elastomer modified; ductile–brittle transition; yielding; strain energy release rate; Charpy impact strength)

INTRODUCTION

Great effort has been devoted in the last decade to improving the impact toughness of polypropylene (PP) by both copolymerization with ethylene and blending with elastomers. The extensive development of particulate filled and short glass fibre reinforced PP has further emphasized the problem of toughening PP. In semicrystalline polymers under common conditions, shear yielding is the main energy dissipation process during fracture[1–4]. The amount of dissipated energy is proportional to the extension of a plastic zone in front of the crack tip whose size depends on the yield strength of the material. The principal effect of elastomer inclusions on the yield strength of semicrystalline polymer blends can be described using Ishai and Cohen's model for the kinetics of yielding of a material containing spherical inclusions[1]:

$$\sigma_y = (kT/v)(1 - 1.21 v_e^{2/3})(\ln \dot{\varepsilon}/A + \Delta H/kT) \qquad (1)$$

where σ_y is the yield strength, k is the Boltzmann constant, T is the absolute temperature, v is the activation volume, $\dot{\varepsilon}$ is the strain rate, ΔH is the activation enthalpy and A is a constant for a given matrix. The increase of the elastomer volume fraction v_e causes a decrease in the yield stress and, since the crack tip plastic zone extension is inversely proportional to σ_y, an increase in plastic zone size. This leads to an enhancement of the energy dissipation and, thus, an increase in the strain energy release rate G for the system. An increase in the strain rate or a decrease in the temperature leads to an increasing yield strength, a reduction of the crack tip plastic zone size and a reduction of G at high crack speed or low temperature.

The concentration, size, shape and modulus of the inclusions, the morphology of the PP matrix and the nature of the applied forces all affect the mode of failure of the material. Of critical importance is an understanding of the nature of the transition from a brittle to a ductile mode of failure[5]. The term brittle–ductile transition is used to describe the sudden change from brittle to ductile behaviour or vice versa. This transition, observed at both low and high deformation rates[6–14], occurs in both amorphous and semicrystalline polymers; however, the mechanisms of energy dissipation vary from material to material. In elastomer filled systems with poor interfacial adhesion, elastomer inclusions act as holes, reducing the matrix effective cross-section and causing local stress concentrations. This reduces the stress necessary for local cold flow and introduces additional deformation mechanisms for dissipating mechanical energy or relieving constraints near the crack tip. Many explanations have been proposed for the brittle–ductile transition mechanism.

Wu[15] found that there exists a critical interparticle distance (i.e. a critical matrix ligament thickness T_c)

*To whom correspondence should be addressed
†ISRIM, Terni, Italy

0032-3861/93/081684-11

below which a rubber modified semicrystalline nylon exhibits a sudden increase in the notched Izod impact strength. The critical ligament thickness T_c was interpreted as the distance at which there is a transition from plane strain (PSN) to plane stress (PSS) behaviour, thereby reducing the critical stress for matrix yielding to about half that required in plane strain. Although the concept is generally accepted, Wu's explanation is not fully satisfactory since the transition occurs at an experimental value of ligament thickness of the order of a thousand times greater than the predicted value[16]. Wu's explanation also assumes that particle radii are much bigger than the crack tip curvature. However, in common toughened semicrystalline polymers, the size of the particles is of the same order as the crack tip curvature (1 μm). Blends of equivalent composition with smaller particles were reported tougher than those with bigger inclusions. Experimental observations by Borggreve *et al.*[6,7] supported the idea of a crucial role of ligament thickness. Since the yield stress is the parameter that controls the ability of the matrix to dissipate mechanical energy, the fracture resistance was correlated to the interconnectivity of microvolumes of an easy-to-yield matrix within the crack tip plastic zone[17].

Sjoerdsma[18] has proposed an alternative model using the concept of interacting stress and percolation theory. He pointed out that the material becomes brittle when the probability of finding an uninterrupted span of non-yielded matrix between the upper and lower bounds of the crack tip plastic zone exceeds a critical value. Contrary to the model proposed by Wu[15], the local yielding was assumed to be caused by the overlap of the local stress fields near elastomer particles, rather than a PSN to PSS transition. This assumption led to the existence of a critical interparticle distance, with spatial packing of inclusions being a primary variable controlling the connectivity of yielded zones. Accurate determination of the stress fields at commercially useful elastomer contents requires calculation of interparticle interactions as well as quantification of changes of matrix morphology due to the presence of the elastomer[19–23].

The use of PP as a matrix for composites has raised the question of improving PP adhesion towards common fillers and reinforcements (glass, calcium carbonate, metal hydroxides, mica, etc.). To enhance the polarity of PP, grafting with a polar monomer such as maleic anhydride is commonly utilized to form grafted polypropylene (MPP). However, there is a lack of published information about the effect of grafting on the mechanical behaviour of MPP and MPP based binary blends. Grafting of polar monomers to ethylene-propylene random copolymer rubber (EPR) is currently proposed as a means of controlling the ternary blend PP/EPR/filler phase morphology[24,25].

The objective of this work is to study the effects of EPR elastomer on the deformation and impact behaviours of PP homopolymer and a random copolymer of PP with ethylene. The effect of grafting maleic anhydride to either PP or EPR on the mechanical behaviour of blends with an unmodified second polymer component was also investigated.

EXPERIMENTAL

Commercial PP homopolymer and a random copolymer containing 2% ethylene and a maleic anhydride grafted PP were used as matrices (*Table 1*). An amorphous EPR, Dutral CO054 (Himont, Italy), containing 60 mol% Et (glass transition temperature, $T_g = -60°C$; $M_w = 180\,000$) and an EPR containing 1.5 wt% grafted maleic anhydride (MEPR) were used as impact modifiers. A two-step mixing procedure was used. An EPR/PP master batch containing 30 vol% PP was first prepared and then mixed with additional PP in a PLE 651 Brabender Plasticorder (Chamber W-50-H, charge 48 ml, 210°C, 50 rev min^{-1}, 10 min) to reach a required EPR volume fraction. Master batching with a blend containing 30 vol% PP improves the elastomer dispersion in PP compared to mixing the PP with pure elastomer. This is a direct result of the morphology of the blend. Sheets were compression moulded from the compounds at 210°C. Specimens cut from the sheet were annealed at 114°C for 90 min and then slowly cooled at 5°C min^{-1}. A sharp notch with a radius of 2 μm was machined into each specimen with lengths varying from 1 to 5 mm using a microtome and diamond knife.

A Zwick Impact Pendulum (impact speed 2.6 m s^{-1}) was used to perform Charpy notched impact tests at temperatures of −20 and 0°C on SEN specimens

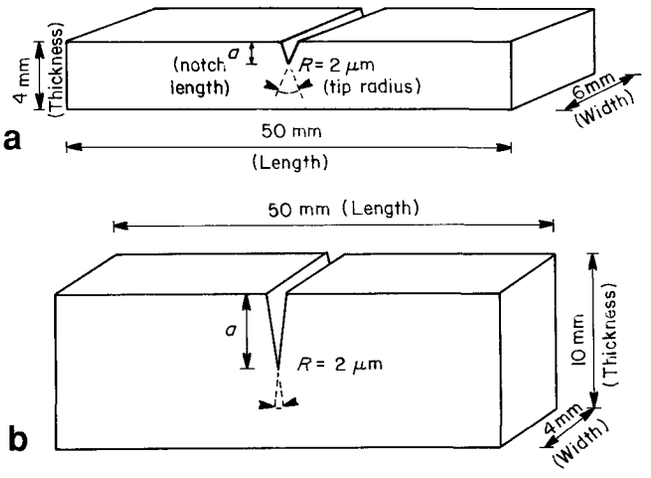

Figure 1 Specimen geometry for measurements of (a) Charpy notched impact strength and (b) strain energy release rate

Table 1 Characteristics of the polymers used as matrices

Polymer	Modulus (GPa)	Yield strength[a] (MPa)	Break strain[a] (%)	NIS[b] (kJ m^{-2})	G_{1c}[c] (kJ m^{-2})
PP homopolymer	1.8	36.4	1060	1.8	1.9
PP copolymer	1.5	24.1	1000	4.3	2.0
Maleated PP (MPP)	2.0	39.0	80	1.6	1.9

[a] Strain rate 3 min^{-1}
[b] At −20°C, Charpy test, impact speed 2.6 m s^{-1}
[c] At 0°C, impact speed 2.6 m s^{-1}

($6 \times 4\,mm^2$ cross-section). The specimen geometry is illustrated in *Figure 1*. The strain energy release rate, G_c', was determined from the slope of the plot of measured fracture energy U *versus* $BD\Phi$, where B is thickness, D is width and Φ is a geometric factor that is a function of the ratio (a/W)[36]. Tensile tests were performed on dog-bone specimens using an Instron 4302 Universal tensile machine at a cross-head speed of $3\,min^{-1}$. Dynamic elastic moduli were measured with a PL DMTA MkII (Polymer Sciences, UK) at 1 Hz and a heating rate of $3°C\,min^{-1}$. Experimental errors were calculated from five specimens for tensile and dynamic mechanical tests and from 10 specimens for impact tests. An AMRAY scanning electron microscope was used for observations of fracture surfaces. The surfaces were prepared by breaking notched specimens in liquid nitrogen. Before coverage with a gold layer, the fracture surfaces were etched for 1 min in boiling n-heptane to remove the elastomer.

RESULTS AND DISCUSSION

Tensile modulus

A decrease of modulus with an increase of the elastomer content was observed for the four PP/elastomer combinations studied (*Figure 2*). The average deviations based on five specimens were of the order of 5%. Chemical modification of the incorporated EPR (MEPR) or the PP (MPP) did not cause any significant difference in the concentration dependence of the elastic modulus. A higher degree of crystallinity in maleated PP (MPP) resulted in higher values of the modulus for MPP based blends.

The model of Kerner was employed to describe the concentration dependence of elastic modulus[26]:

$$E^{rel} = (1 + ABv_{EPR})/(1 - Bv_{EPR}) \qquad (2)$$

$$A = (7 - 5\nu_m)/(8 - 10\nu_m) \qquad B = (E_e/E_m - 1)/(E_e/E_m + A)$$

PP and EPR are immiscible[34] and the moduli ratio E_{EPR}/E_{PP} is 1/600. Poisson's ratios for PP and EPR are 0.33 and 0.4997, respectively. The parameters A and B of the Kerner equation were calculated using EPR as inclusions in one case and matrix in the other since a phase inversion from a dispersed to a continuous phase appears to occur above 50 vol%. The transition region occurred between 30 vol% and 60 vol% EPR. However, the significantly higher modulus of the blend at 70 vol% EPR, compared to the prediction based on EPR matrix and PP inclusions, indicated that the PP still preserves partial continuity. This was confirmed by SEM observations, revealing that the lower viscosity polymer (PP) tends to form a secondary continuous phase even as a minor component. Additionally, it has been found that the presence of EPR affects the morphology of PP[22]. The dispersed phase appears to engulf the growing fibrils of the PP spherulites. Some of the spherulite centres were occupied by EPR particles, confirming the likelihood of some nucleation of PP homopolymer on EPR surfaces[4]. At the same time, addition of EPR resulted in a less regular spherulite texture with less sharp spherulite boundaries. The average spherulite diameter decreased from 100 μm in PP homopolymer to ~ 40 μm after adding 10 vol% EPR. Further addition of elastomer caused no significant reduction of spherulite diameter.

Dynamic moduli

The damping capacities of PP and its blends with EPR as a function of temperature are shown in *Figure 3*. Two main relaxation regions are observed. The transition around $-50°C$ is the glass transition of EPR. Its relative magnitude increases with increase in EPR content. The relaxation region around 0°C is the glass transition of

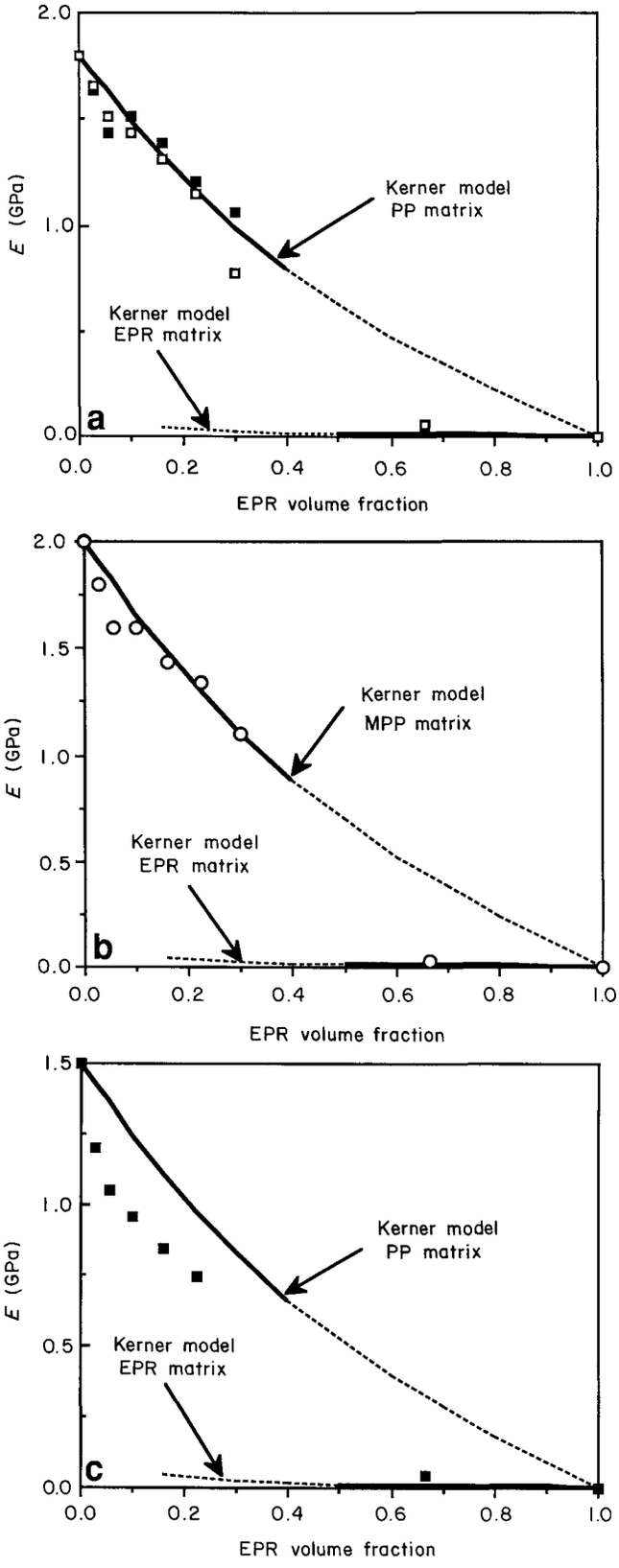

Figure 2 Concentration dependence of Young's modulus E at 23°C for (a) PP homopolymer with EPR (■) or MEPR (□), (b) MPP/EPR (○) and (c) PP copolymer/EPR (■)

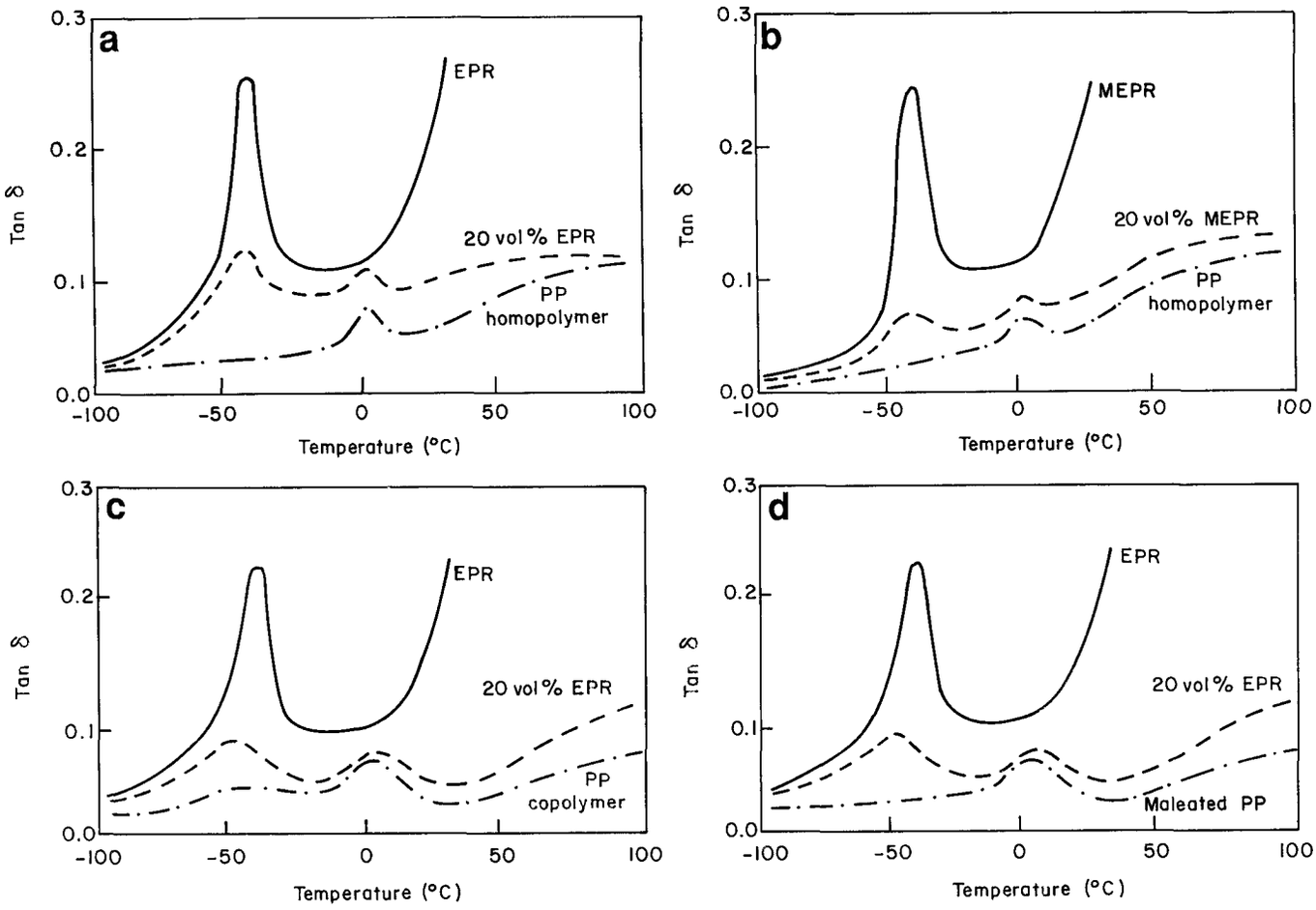

Figure 3 Temperature dependence of the loss tangent, tan δ (1 Hz, 3°C min^{-1}) for (a) PP homopolymer/EPR, (b) PP homopolymer/MEPR, (c) PP copolymer/EPR and (d) maleated PP/EPR

PP. The relative magnitude of this loss peak is reduced with increasing EPR content. The positions of both peaks are neither changed by the blending nor dependent on the EPR content. Thus, one can deduce that there is no significant bulk interaction between PP and EPR[35]. As can be seen in *Figure 3*, EPR has a considerably higher damping capacity than PP, resulting in lower damping capacities for the blends relative to pure EPR.

Yielding and ductility

Yield strength. The yield strength and ductility of PP/EPR blends are controlled by a competition between crack formation and plastic deformation through shear yielding[16,27]. The stress concentration introduced by EPR particles reduces both the macroscopic shear yield strength and the stress at which cracks form. In addition, the lack of 'adhesion' between PP and EPR prevents the rubber particles from effectively controlling craze propagation.

Due to the poor adhesion and low moduli ratio, there is little or no stress transfer from the matrix to the elastomer particles. Elastomer inclusions in the blend behave, above their T_g of −50°C, like voids. Additional increase of the void volume fraction due to particle dewetting during loading reduces significantly the tangent modulus of the blend and thus affects the shape of the stress–strain curve. Under these conditions, a PP/EPR blend can be viewed as a porous medium where the EPR particles act as a controlled dispersion of voids. The effect

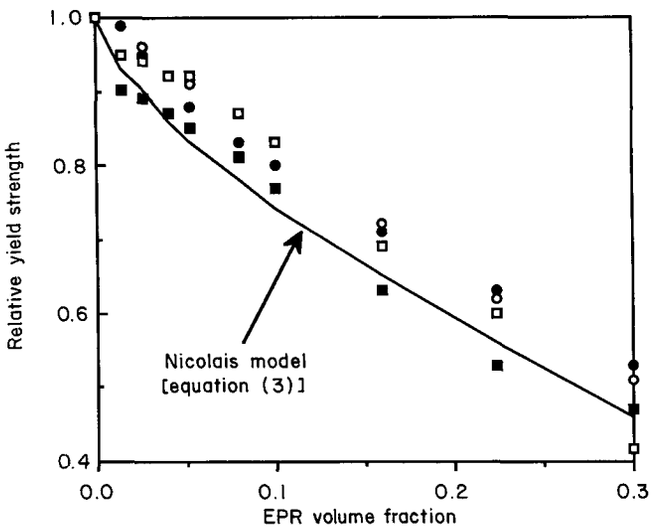

Figure 4 Concentration dependence of the relative yield strength for all blends studied compared to the prediction based on equation (3): PP homopolymer/EPR (○); PP copolymer/EPR (●); maleated PP/EPR (■); PP homopolymer/maleated EPR (□)

of increasing the EPR concentration is a decrease in the overall yield strength (*Figure 4*) caused by the reduction of the effective matrix cross-section and consequent stress concentration. The engineering yield strength of the blends, σ_y^{bl}, as a function of elastomer concentration can be described using the model proposed by Nicolais and Narkis[28]:

Table 2 Yield strength and relative yield strength of PP homopolymer and copolymer based blends

EPR content	Yield strength (MPa)		Relative yield strength	
	Homopolymer	Copolymer	Homopolymer	Copolymer
0.00	36.4	24.1	1.00	1.00
0.05	33.6	21.2	0.91	0.88
0.10	30.6	19.3	0.83	0.80
0.15	26.6	17.3	0.72	0.71
0.20	24.7	15.9	0.67	0.66
0.25	21.0	14.2	0.57	0.59
0.30	19.9	13.3	0.54	0.55

$$\sigma_y^{bl} = \sigma_y^m(1 - 1.21 v_{EPR}^{2/3})S \quad (3)$$

where S is a stress reduction factor varying with the filler volume fraction between 1 and 0.2[21,29]. For the case of a ductile matrix, $S=1$ and the effects of local stress concentration are not important since they do not cause the instantaneous failure of the material.

D.s.c. and density measurements indicate that the PP homopolymer contains ~56 wt% of the crystalline phase while the copolymer contains only 40 wt%. The lower degree of crystallinity accounts for the lower yield strength of the copolymer (*Table 2*). The yield strength relative to the pure component, however, was more or less constant, as shown in *Table 2*, indicating that the concentration dependences are quite similar for both matrices. Grafting maleic anhydride onto EPR did not change the elastomer modulus or its adhesion to PP and, hence, the magnitude of the stress fields around MEPR inclusions remains unchanged. As expected, PP/MEPR blends exhibited the same yield behaviour as the PP/EPR blends.

The PP modified by grafting of maleic anhydride contains 66 wt% crystalline phase, compared to 56 wt% for PP homopolymer and, at the same time, has poorly developed spherulites and crystallites[30]. The absolute value of the yield strength is higher than that for PP homopolymer. However, the relative yield strength of its blends with EPR was significantly lower than that of PP homopolymer based blends due to lower ductility and consequently a bigger effect of stress concentration. The effect of matrix ductility on the failure of blends can be evaluated by introducing a ductility parameter:

$$\mu = (\varepsilon_{br} - \varepsilon_y)/\varepsilon_y \quad (4)$$

where ε_{br} and ε_y are the strain at break and yield strain, respectively. At low elastomer content (up to 3–5 vol%), $\mu < 3$ and microzones of plastically deformed material around adjacent inclusions are not connected. The material behaves in a brittle manner and the effect of a stress reduction factor has to be utilized [$S < 1$ in equation (3)]. At higher elastomer volume fractions, the probability of connecting yielded microzones around adjacent particles increases and the effect of stress concentration is not detrimental and the material fails in a ductile manner. Within the interval from 5 to 15 vol% EPR, $\mu > 3$ and experimental data are in good agreement with the prediction using $S = 1$ (*Figure 4*). A further increase of the elastomer volume fraction leads to the decrease of the relative yield strength of the blend caused by microcracks due to intensive interactions of yielded microzones.

When adhesion is poor and the moduli ratio is low, stress is concentrated at the inclusion equator rather than the poles. The stress concentration in this region causes localized plastic deformation or microcavitation in the direction nearly perpendicular to the direction of applied load. The magnitudes of shear yielding and crazing are a function of temperature and strain rate[3]; the local state of stress is a function of EPR volume fraction, spatial packing of the inclusions and the morphology of the matrix. Using simple cubic space packing and assuming monodisperse inclusions, one can plot the dependence of the relative yield strength *versus* ligament thickness (*Figure 5*). There is a significant reduction of the yield strength for a ligament thickness smaller than the particle diameter. This reduction can most probably be ascribed to an overlap of the local stress fields. The significant drop in yield strength for the PP based blends occurs at a corresponding particle loading of ~5–10 vol%.

Elongation at break. The elongation at break, ε_{br}, was found to be influenced by both the nature of the matrix and the particle volume fraction (*Figure 6*). A comparison of the behaviour of unfilled PP and a blend with 30 vol% EPR indicates that the generation of voids around the elastomer particles eliminated the tendency of the matrix to strain harden. Extensive stress whitening in all blends was observed before the general yield point. Such a pre-yielding phenomenon was not observed in the PP homopolymer and only slightly in the copolymer under the same test conditions. This suggests that it was primarily due to the formation of cavities near the EPR inclusions. Because there is no means of restricting microcrack growth in these materials, catastrophic cracks develop rapidly and lead to a decrease in the strain at break of blends compared to that of PP homopolymer.

In PP copolymer based blends, multiple shear banding around EPR particles becomes the most important energy absorbing process because of the lower yield strength compared to that for PP homopolymer. The effect of particle dewetting is suppressed in the copolymer through the development of shear bands that tend to inhibit microcrack growth and effectively prevent an individual crack from becoming large enough to form an unstable crack. This mechanism increases the ductility at low elastomer content when the interactions among shear bands are minimal. At higher elastomer content, however, the shear bands interact, microcracks develop at the loci of high mechanical constraints and, consequently, the ultimate strain is reduced. The extent of plastic flow before failure is evident in the SEM micrograph of the fracture surface of a copolymer based blend containing 15 vol% EPR (*Figure 7*).

There is no significant effect on the stress–strain response of the blend caused by grafting maleic anhydride

onto the elastomer. On the other hand, as shown in *Figure 6b*, an increase in the relative elongation at break of up to one order of magnitude was observed when maleic anhydride was grafted onto the PP homopolymer

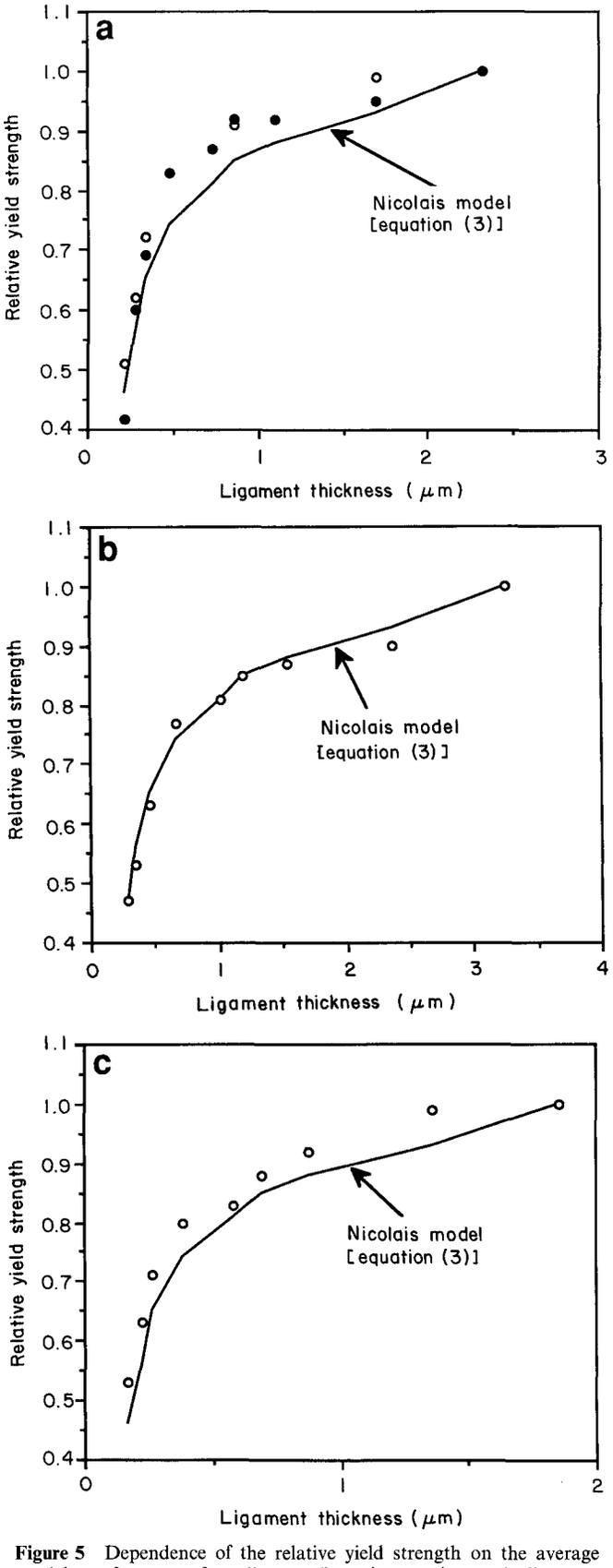

Figure 5 Dependence of the relative yield strength on the average particle surface-to-surface distance (i.e. microscopic matrix ligament thickness) for (a) PP homopolymer/EPR (○) and PP homopolymer/MEPR (●), (b) maleated PP/EPR (○) and (c) PP copolymer/EPR (○)

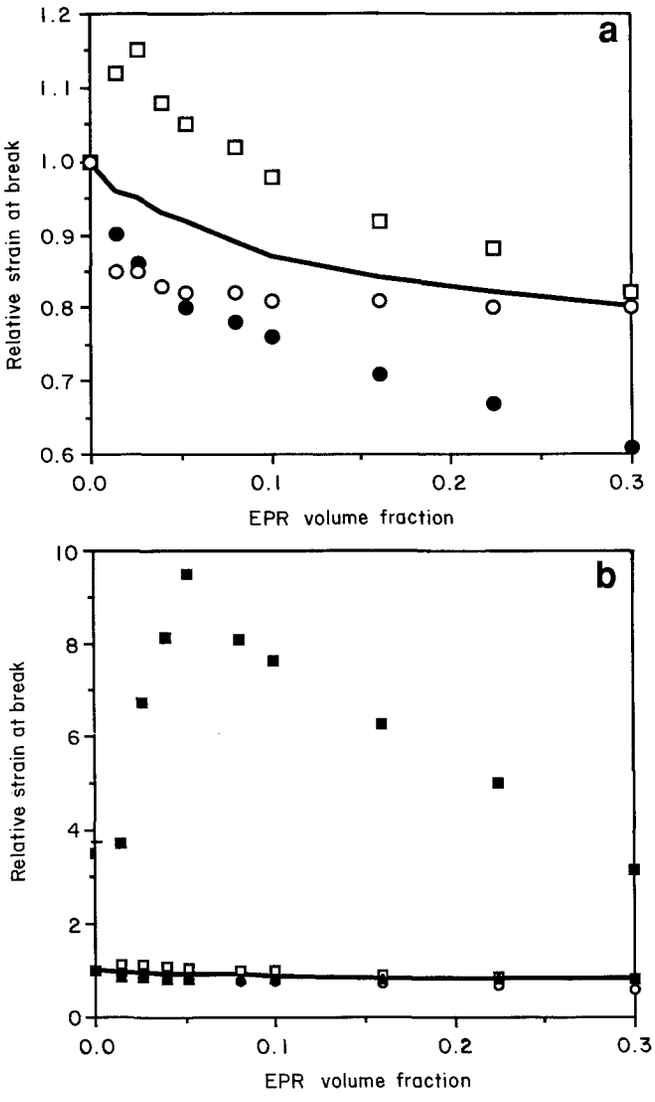

Figure 6 Concentration dependence of the relative strain at break compared to the prediction based on the Nielsen model for 'zero' adhesion (——) at 23°C. (a) MPP/EPR blends are excluded: PP homopolymer/EPR (●); PP copolymer/EPR (□); PP homopolymer/maleated EPR (○). (b) MPP/EPR blends are included: maleated PP/EPR (■); PP homopolymer/EPR (○); PP homopolymer/maleated EPR (▲); PP copolymer/EPR (□)

(even though the absolute values of ε_{br} for MPP/EPR blends were in all cases lower than those for PP homo- and copolymer based blends). Moreover, the concentration dependence of strain at break of the MPP/EPR blend was not monotonic, but rather had a well pronounced maximum at 6 vol% EPR. EPR has significantly less effect on the crystalline structure of MPP than on that of common PP homopolymer due to the significantly different morphology of MPP. The MPP contains only ~10 wt% more crystalline phase than PP homopolymer; however, its spherulites are an order of magnitude smaller (average spherulite diameter 10 μm) than those for common PP and more poorly developed, with thinner and less coherent lamellae[22]. It is believed that these differences are caused by significantly different kinetics of crystallization and lower molecular weight[31]. Increased crystallinity raises the modulus and yield strength of MPP and reduces the yield strain and strain at break. Due to the small size of spherulites, EPR does not further reduce their size in MPP in contrast to the reduction reported for common PP homopolymer by

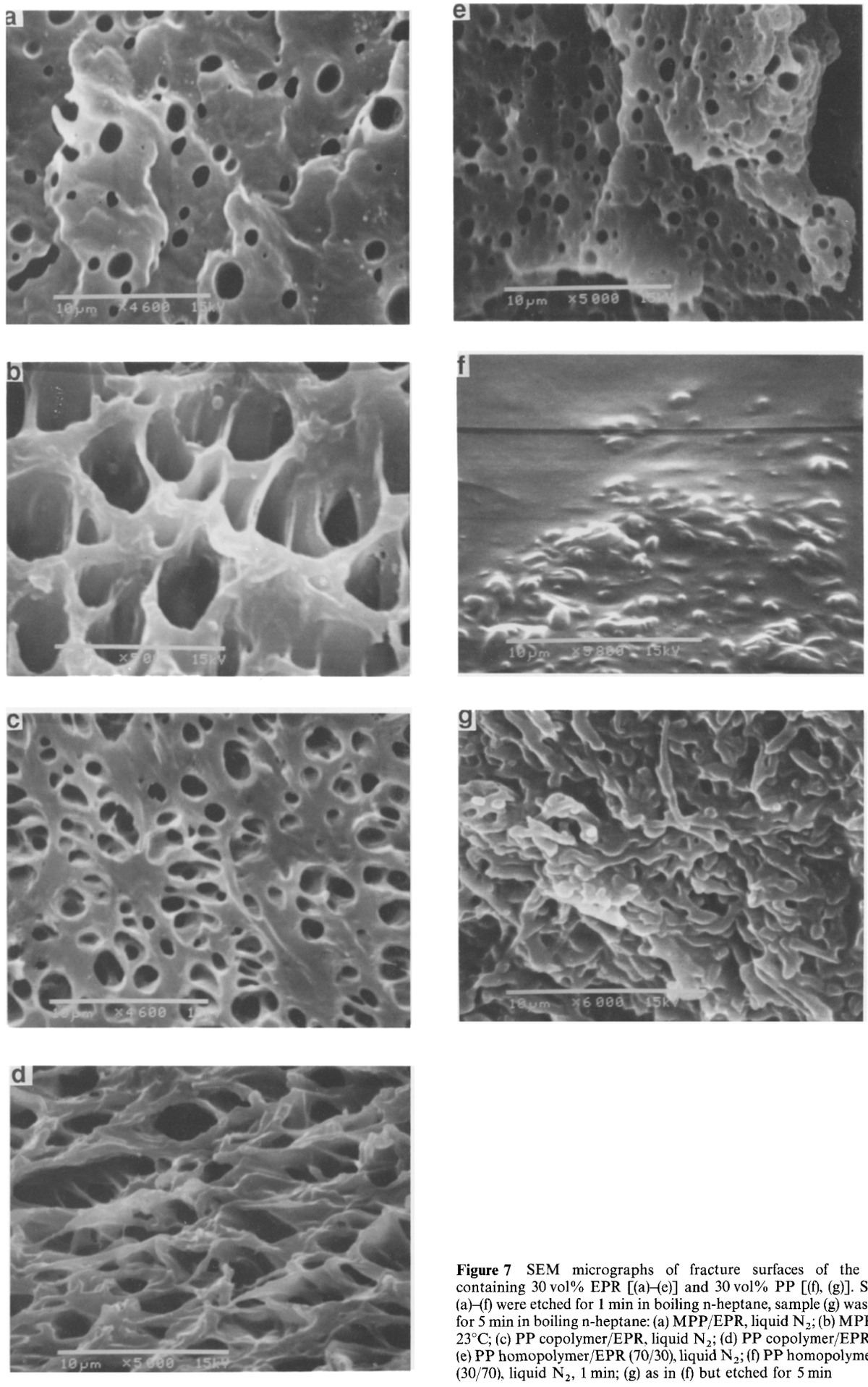

Figure 7 SEM micrographs of fracture surfaces of the blends containing 30 vol% EPR [(a)–(e)] and 30 vol% PP [(f), (g)]. Samples (a)–(f) were etched for 1 min in boiling n-heptane, sample (g) was etched for 5 min in boiling n-heptane: (a) MPP/EPR, liquid N_2; (b) MPP/EPR, 23°C; (c) PP copolymer/EPR, liquid N_2; (d) PP copolymer/EPR, 23°C; (e) PP homopolymer/EPR (70/30), liquid N_2; (f) PP homopolymer/EPR (30/70), liquid N_2, 1 min; (g) as in (f) but etched for 5 min

Jang *et al.*[4]. Introduction of subcritical elastomer inclusions in the brittle matrix, enabling localized yielding due to the stress concentration, allows the small crystallites with a high density of tie molecules to undergo easier cold drawing.

Impact behaviour

Generally, the energy absorbed during impact is dissipated by yielding, crazing, creation of new crack surfaces and the kinetic energy of the broken specimen. These processes, except for the kinetic one, are controlled by the material properties, the state of stress, the boundary conditions and the method of loading. Overall, the dissipative processes in the inelastic region are the most important source of toughness of a material. Failure of the material can be characterized by two quantities: an energy of crack initiation, characterized by the strain energy release rate G_c, and the resistance to crack propagation, characterized by standard notched impact strength (NIS). The observed toughness comes from two distinct contributions: one in the interior of the specimen where a state of plane strain (PSN) exists; and the other near the edges of the specimen where a plane stress (PSS) condition exists. The relative importance of the two contributions is related to the sizes of the crack tip plastic zones in the corresponding states. The size of the plastic zone in the plane stress state is proportional to the ratio of the stress intensity factor K_{2c} in PSS and the yield strength of the material σ_y[32]:

$$r_y=(1/2\pi)(K_{2c}/\sigma_y)^2 \quad (5)$$

If $2r_y$ is equal to the specimen width W_c, the whole sample cross-section is in the PSS condition and the measured value of the fracture toughness is designated as the PSS stress intensity factor K_{2c}. This upper bound for the stress intensity factor is thus approximated by:

$$K_{2c}=\sigma_y(W_c\pi)^{1/2} \quad (6)$$

The most conservative value of the stress intensity factor, the plane strain value K_{1c}, is obtained when the whole specimen cross-section is in the PSN state. When the stress–strain response to fracture is linearly elastic K_{1c} can be related to K_{2c} by the following approximation[33]:

$$K_{1c}=K_{2c}(1-2\nu) \quad (7)$$

where ν is Poisson's ratio. The strain energy release rate G_c is related to the stress intensity factor K_c by the equation:

$$K_{Ic}^2=G_{Ic}E \quad (8)$$

in the PSS state and by:

$$K_{Ic}^2=G_{Ic}E/(1-\nu^2) \quad (9)$$

in the PSN state. When dealing with crack propagation involving a large energy dissipation through a fully plastically deformed volume of material, it is common practise to replace the strain energy release rate G_c with the J-integral[12,33,34] to indicate that non-linear energy dissipative terms are included ($G_c=J$ in the elastic case). J can be estimated from the total energy adsorbed during the impact event, U, and the ligament area A:

$$J=2U/A \quad \text{and} \quad A=(B-a)W \quad (10)$$

where B is the sample width and a is the crack length. In an intermediate condition, when the size of the plastic zone is not negligible but is not as large as the ligament length, i.e. $W_c=2r_y<(B-a)$, an upper limit for J_{Ic} can be approximated by $J_{Ic}=2G_{Ic}$.

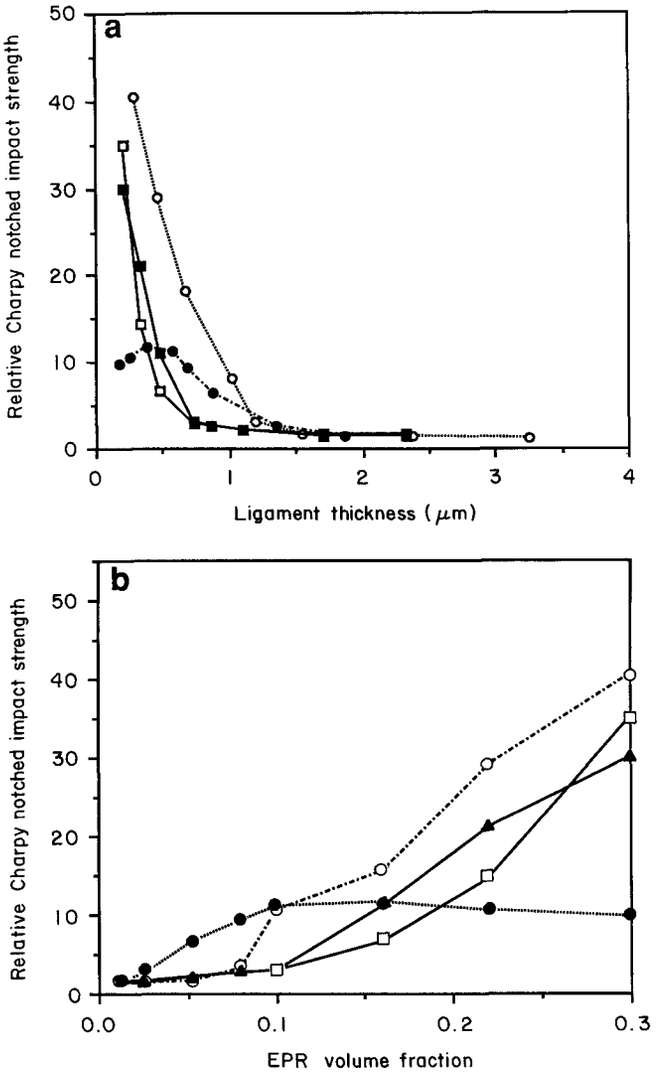

Figure 8 Dependence of relative Charpy notched impact strength at −20°C on (a) the average particle surface-to-surface distance and (b) the elastomer volume fraction: PP homopolymer/EPR (□); PP copolymer/EPR (●); maleated PP/EPR (○); PP homopolymer/EPR (■); PP homopolymer/maleated EPR (▲)

Figure 8 illustrates the effects of EPR volume fraction and matrix ligament thickness calculated using a simple cubic packing geometry on the relative impact strength of the blends. The results can be converted to values of relative strain energy release rate as shown in *Figure 9*. Due to the viscoelastic character of the matrix, yield strength increases with the increase in strain rate. Thus, yield strength data measured at low strain rate cannot be used for the analysis of an impact event. However, the relative change of the yield strength with the volume fraction of inclusions is independent of the strain rate[1]. Assuming this, one can measure the yield strength of PP at the impact strain rate ($2.6\,m\,s^{-1}$) and then use the relative yield strength measured at low rate tensile test for the analysis of relative strain energy release rate measured in an impact experiment. This approach assumes one failure mechanism over the extrapolated range of strain rates. Even if not fully satisfactory, the relative error in the calculations is probably in the range of experimental standard deviation.

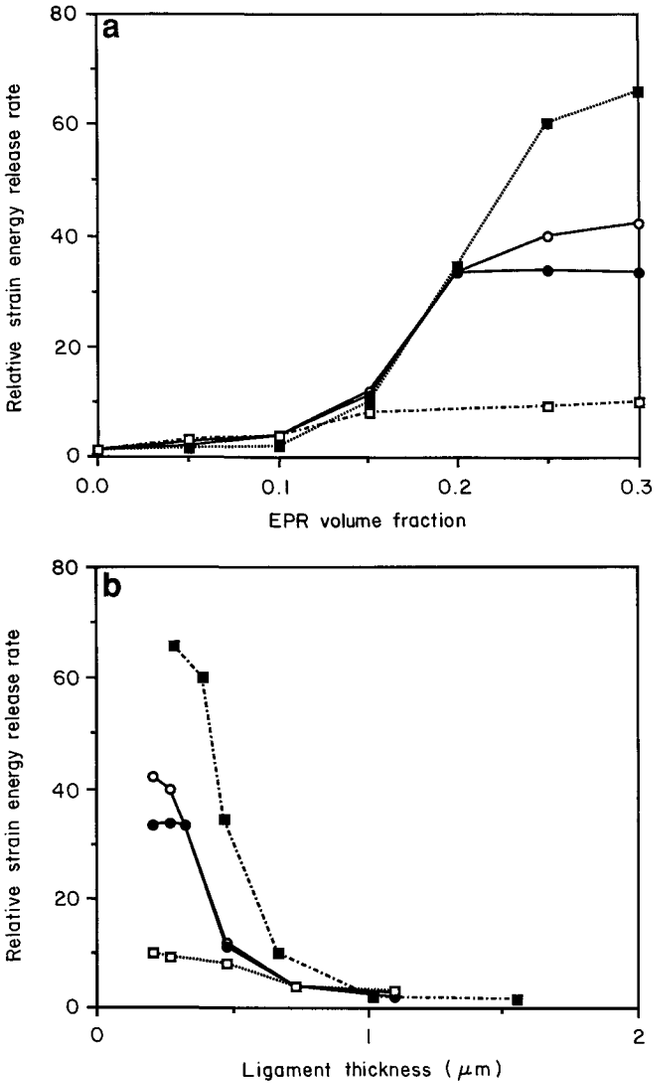

Figure 9 Dependence of the relative strain energy release rate at 0°C on (a) the elastomer volume fraction and (b) the average particle surface-to-surface distance: PP homopolymer/EPR (○); PP homopolymer/maleated EPR (●); PP copolymer/EPR (□); maleated PP/EPR (■)

As previously noted, the EPR inclusions induce a reduction of the yield stress of the blends. This leads to a further increase in the PSS contribution to G_c and a greater involvement of the inelastic dissipative processes. The experimental concentration dependence of the strain energy release rate, $G_{Ic,bl}$, relative to the value of $G_{Ic,m}$ of the matrix, for the PP/EPR blends is in accordance with the experimental observations of Fernando and Williams[10,11]. For these types of blends it has been observed that the PSN stress intensity factor K_{1c} represents a minimum value for crack initiation in the matrix and is independent of the elastomer volume fraction:

$$K_{1c}^{bl} = K_{1c}^{m} \tag{11}$$

Under common experimental conditions, the measured stress intensity factor K_c can be estimated as a function of K_{1c}, K_{2c}, σ_y and the sample thickness W[11]:

$$K_c = K_{1c} + (1/\pi W)(K_{2c}/\sigma_y)^2(K_{2c} - K_{1c}) \tag{12}$$

After simple rearrangements of equation (12), the dependence of the measured strain energy release rate relative to that of the matrix, $G_{c,bl}^{rel}$, on the elastomer volume fraction can be expressed by equation (A3) (see Appendix):

$$G_{c,bl}^{rel} = G_{c,bl}/G_{c,m} = \{\alpha_m[1 + (\beta_m \gamma_{bl}/\pi W)/(\sigma_{y,bl}^{rel})^2]\}^2/E_{bl}^{rel} \tag{13}$$

A comparison between equation (13) and the experimental results is shown in *Figure 10*. For elastomer volume fractions below 0.05, the size of the plastic zone, $2r_y^{bl}$, is small compared to the dimensions of the specimen. The measured $G_{c,bl}^{rel}$ values are then well described by equation (13) (solid line, *Figure 10*). With increasing elastomer volume fraction, the yield strength $\sigma_{y,bl}^{rel}$ decreases, the size of the PSS plastic zone in the specimen cross-section increases and the contribution of the plane stress value of G_c, i.e. G_{2c}, becomes more and more important.

At a certain elastomer volume fraction, the size of the plane stress region becomes as large as the sample thickness W(i.e. $W_c/W = 2r_y^{bl}/W = 1$). This point is reached in the interval $0.15 < v_{EPR} < 0.20$ and the measured $G_{c,bl}$ values are then better approximated by the relation:

$$J_{c,bl} = 2G_{c,bl} \tag{14}$$

which is plotted as the dotted line in *Figure 10*.

For an elastomer volume fraction greater than 0.2, the size of the yielded region is comparable to the ligament length $(B - a)$. Under these conditions the crack propagates through a fully yielded material and the J-integral exceeds the value of $2G$ predicted by equations (13) and (14). Beyond some critical value of elastomer concentration the mean interparticle distance (i.e. the microscopic ligament thickness envisioned by Wu[15]) becomes smaller than the critical distance required for full connectivity, and the volume of material undergoing plane stress deformation decreases causing a decrease in the strain energy release rate along with continued decreases in the yield strength and elongation at break. This effect appears to occur in both samples of 0.3 elastomer volume fraction shown in *Figure 10*.

Generally, the presence of the elastomer enhances the stability of a growing crack. This is in agreement with a significant reduction of the crack speed as observed by Bramuzzo[12] using a high speed camera and an instrumented impact pendulum. For low elastomer volume fraction, the failure during an impact event is controlled by the crack initiation. This process is determined by the matrix morphology and deformation properties. With an increase of the elastomer content the relative importance of the initiation becomes less than that of the propagation. This can be described by the increase of the values of the measured G_c and Charpy NIS. The observed crack stabilization is caused by the reduction of the external stress necessary to plastically deform the matrix. By reducing the shear yield strength, an extensive shear banding can occur, even at subambient temperatures and high strain rate. At the same time, crazing most probably becomes an additional energy dissipative process, as the craze growth is controlled by the developing shear bands.

CONCLUSIONS

The size, shape and spatial packing of elastomer inclusions have been shown to be the most important factors in controlling the mechanical behaviour of

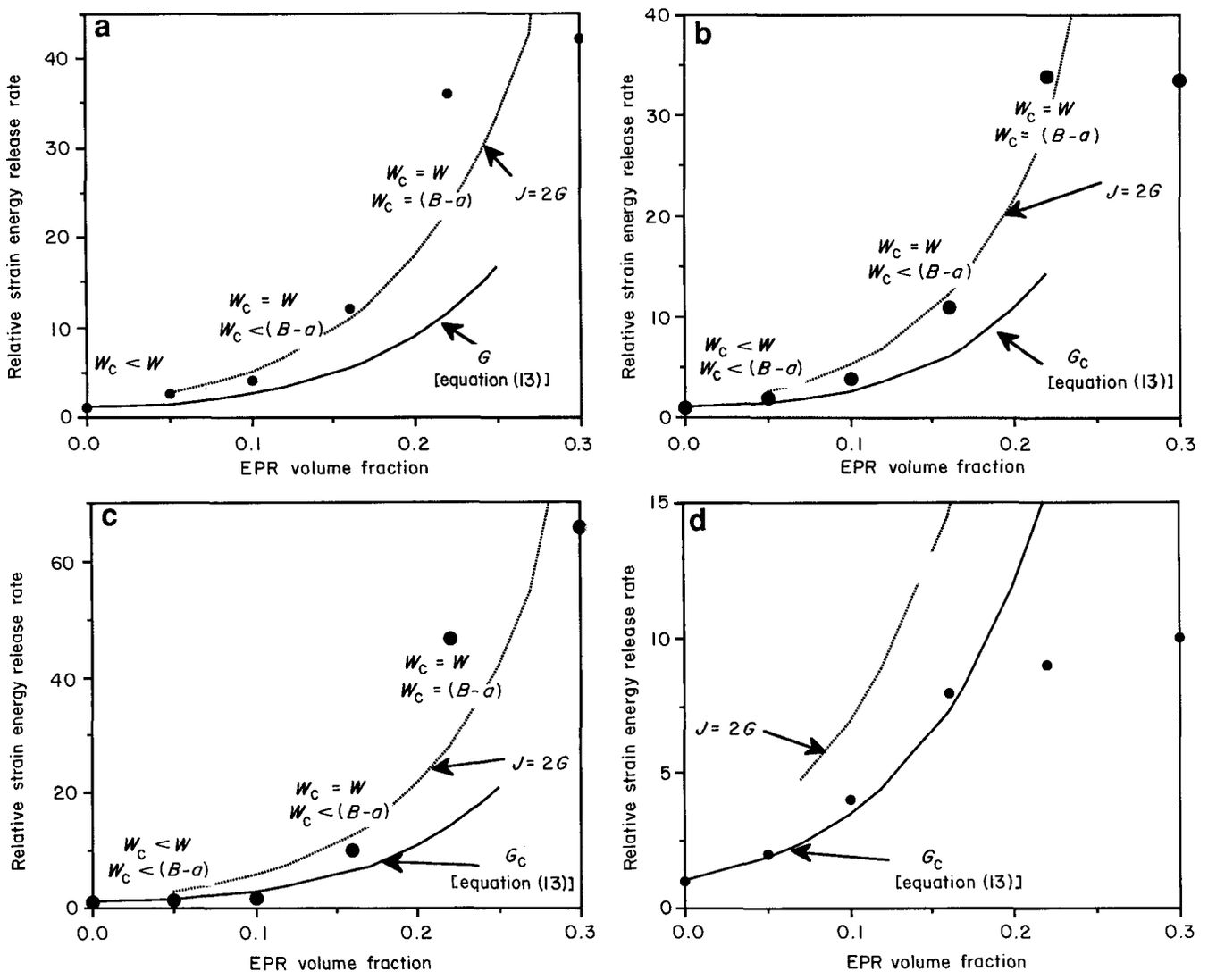

Figure 10 Concentration dependences of the relative strain energy release rate at 0°C compared with that theoretically predicted using equation (13) for (a) PP homopolymer/EPR (●), (b) PP homopolymer/maleated EPR (●), (c) maleated PP/EPR (●) and (d) PP copolymer/EPR (●)

PP/EPR blends. These factors depend strongly on the blending process and, therefore, on the viscosities of the matrix and the elastomer in the melt. PP remains a continuous phase even when it is a minor component. Even though there are visible changes in the morphology of PP in the presence of EPR particles, it does not appear to affect the fracture toughness relative to crack initiation in the matrix phase. Thus, the plane stress and plane strain fracture toughness of the PP/EPR blends remain unchanged when compared to those of pure PP. 'Toughening', observed under the conditions of this study, is due to the reduction of the yield strength and consequent increase of the plane stress contribution to the overall fracture toughness. Since the EPR particles affect the crack growth stability, however, the transition from a brittle mode of failure to a ductile mode occurs at a sample thickness that is a function of the elastomer concentration.

While the observed trends of the dependence of relative impact strength and observed fracture toughness of the blends on the EPR content can be regarded as generally valid, the absolute values obtained are unique for a given blending process as a consequence of the strong effect of the blending process on the mechanical properties of PP/EPR blends.

REFERENCES

1 Bucknall, C. B. *Adv. Polym. Sci.* 1978, **27**, 121
2 Wu, S. *J. Polym. Sci., Polym. Phys. Edn* 1983, **21**, 699
3 Schultz, J. M. *Polym. Eng. Sci.* 1984, **24**, 770
4 Jang, B. Z., Uhlmann, D. R. and van der Sande, J. B. *J. Appl. Polym. Sci.* 1984, **29**, 3409
5 Bucknall, C. B. 'Toughened Plastics', Applied Science, London, 1977
6 Borggreve, R. J. M., Gaymans, R. J., Schnijer, J. and Ingen-Houzs, J. F. *Polymer* 1987, **28**, 1489
7 Borggreve, R. J. M., Gaymans, R. J., Schnijer, J. and Ingen-Houzs, J. F. *Polymer* 1989, **30**, 71
8 Borggreve, J. R. M., Gaymans, R. J. and Eichenwald, H. M. *Polymer* 1989, **30**, 78
9 Borggreve, J. R. M., Gaymans, R. J. and Luttmer, A. R. *Macromol. Chem. Macromol. Symp.* 1988, **16**, 195
10 Fernando, P. L. and Williams, J. G. *Polym. Eng. Sci.* 1980, **20**, 215
11 Fernando, P. L. and Williams, J. G. *Polym. Eng. Sci.* 1981, **21**, 1003
12 Bramuzzo, M. *Polym. Eng. Sci.* 1989, **29**, 1077
13 Jang, B. Z., Uhlmann, D. R. and van der Sande, J. B. *J. Appl. Polym. Sci.* 1985, **30**, 2485
14 Wu, S. *Polymer* 1985, **26**, 1855
15 Wu, S. *J. Appl. Polym. Sci.* 1988, **35**, 549
16 Williams, J. G. 'Fracture Mechanics of Polymers', Ellis Horwood, Chichester, 1984, p. 151
17 Margolina, A. and Wu, S. *Polymer* 1988, **29**, 2171
18 Sjoerdsma, S. D. *Polym. Commun.* 1989, **30**, 106
19 Broutman, L. J. and Panizza, G. *Int. J. Polym. Mater.* 1971, **1**, 95

20 Greenwood, J. A. *Int. J. Mech. Sci.* 1989, **31**, 219
21 Guild, F. J. and Young, R. J. *J. Mater. Sci.* 1989, **24**, 2454
22 Jang, B. Z., Uhlmann, D. R. and van der Sande, J. B. *J. Appl. Polym. Sci.* 1984, **29**, 4377
23 Matsuo, M., Wang, T. T. and Kwei, T. K. *J. Polym. Sci. A2* 1972, **10**, 1085
24 Kolarik, J., Jancar, J., Lednicky, F. and Pukanszky, B. *Polym. Commun.* 1990, **31**, 201
25 Matonis, V. A. *Polym. Eng. Sci.* 1969, **9**, 100
26 Nielsen, L. E. 'Mechanical Properties of Polymers and Composities', Vol. 2, Marcel Dekker, New York, 1972, p. 394
27 Friedrich, K. *Mater. Res. Soc. Symp. Proc.* 1987, **79**, 357
28 Nicolais, L. and Narkis, M. *Polym. Eng. Sci.* 1971, **11**, 174
29 Jancar, J., DiAnselmo, A. and DiBenedetto, A. T. *Polym. Commun.* 1991, **32**, 367
30 Jancar, J. *J. Mater. Sci.* 1989, **24**, 4268
31 Pospisil, L., Jancar, J. and Rybnikar, F. *J. Mater. Sci. Lett.* 1990, **9**, 495
32 Williams, J. G. 'Fracture Mechanics of Polymers', Ellis Horwood, Chichester, 1984, p. 100
33 Atkins, A. G. and Mai, Y. W. 'Elastic and Plastic Fracture', Ellis Horwood, Chichester, 1985
34 Hashemi, S. and Williams, J. G. *J. Mater. Sci.* 1991, **26**, 621
35 Kolarik, J. *et al. Polym. Compos.* 1986, **7**, 463
36 Williams, J. G. 'Fracture Mechanics of Polymers', Ellis Horwood, Chichester, 1984, p. 245

APPENDIX

The measured stress intensity factor K_c contains two contributions, one (K_{1c}) from the plane strain region and the other (K_{2c}) from the plane stress region. For a given specimen width W, Fernando and Williams[11] proposed a relation between the experimental value of K_c and the limiting values K_{1c} and K_{2c}:

$$K_c = K_{1c} + (1/\pi W)(K_{2c}/\sigma_y)^2(K_{2c} - K_{1c}) \quad \text{(A1)}$$

Assuming $K_{1c,bl} = K_{1c,m}$ and $K_{1c} = K_{2c}(1-2\nu)$, one can rearrange equation (A1) as:

$$K_c = K_{1c}\{1 + [(1/\pi W)(K_{1c}/\sigma_y)^2][2\nu/(1-2\nu)^3]\} \quad \text{(A2)}$$

where ν is Poisson's ratio. The strain energy release rate G_c is approximately equal to K_c^2/E (exactly so in the PSS state), so that equation (A2) can be rewritten in terms of the relative strain energy release rate:

$$G_{c,bl}^{rel} = G_{c,bl}/G_{c,m} = \{\alpha_m[1 + (\beta_m \gamma_{bl}/\pi W)/(\sigma_{y,bl}^{rel})^2]\}^2/E_{bl}^{rel} \quad \text{(A3)}$$

where:

$$\alpha_m = \{1 + [K_{1c,m}^2/(\sigma_{y,m}^2 \pi W)][2\nu_m/(1-2\nu_m)^3]\}^{-1} \quad \text{(A4)}$$

$$\beta_m = (K_{1c,m}/\sigma_{y,m})^2 \quad \text{(A5)}$$

$$\gamma_{bl} = 2\nu_{bl}/(1-2\nu_{bl})^3 \quad \text{(A6)}$$

$$\sigma_{y,bl}^{rel} = \sigma_{y,bl}/\sigma_{y,m} \quad \text{(A7)}$$

$$E_{bl}^{rel} = E_{bl}/E_m \quad \text{(A8)}$$